Multiband Comb-Enabled mm-Wave Transmission

Dhecha Nopchinda, *Member, IEEE*, Zichuan Zhou, *Member, IEEE*, Zhixin Liu, *Senior Member, IEEE*, and Izzat Darwazeh, *Senior Member, IEEE*

***Abstract*— A novel architecture to generate and distribute multiband frequency-synchronized sources is studied through an experimental system for simultaneous transmission at 100 and 112.5 GHz in two of the *W*-band subbands. An electrooptic frequency comb, containing frequency-synchronized sources, was generated OFF-site and distributed to multiple locations using optical fibers of various lengths and total chromatic dispersion. The effect of the dispersion is studied and demonstrated experimentally. At each site, the optical comb is converted to the equivalent electrical comb (e-comb) using a photodiode (PD) without prior optical filtering. Subsequently, three different frequency-synchronized sources are extracted from the e-comb and used as oscillator and clock sources of the local mm-wave transmitters (TXs). To further provide synchronization between the mm-wave TXs and the remote mm-wave receivers (RXs) without access to the comb, the extracted clock signal at 6.25 GHz was also broadcasted over-the-air to the RXs. The optical comb was generated using the electrooptic technique whereby only one electrical oscillator, determining the phase noise characteristics, is required. The architecture thus provides the capability to generate multiple frequency-synchronized sources, with enhanced phase noise performance suitable for mm-wave transmission, across multiple sites and locations. The performance of the architecture is characterized at varying optical fiber lengths as the parameter of interest. Comparisons to electronic oscillators are also provided. Thus, this work is an experiment demonstration, with theoretical analysis, on the impact of the o-comb distribution and subsequent direct generation of the e-comb in the proposed architecture. In particular, the work demonstrates how chromatic dispersion affects the power and phase noise of the extracted sources and subsequently the mm-wave system performance as a whole.**

***Index Terms*— Data transmission, frequency comb, frequency generation, frequency synchronization, microwave photonics, millimeter wave, multiband transmission, phase noise.**

I. Introduction

THE applications envisioned for the emerging 5G and the future 6G network entail stringent requirements on the performance of wireless systems. These include the capability to provide large data capacities for virtual realities, connected cars, and IoT infrastructures [1]. With the various frequency bands defined in the mm-wave space, the simultaneous utilization of these bands, a multiband mm-wave link, is a promising solution to fulfill these requirements by using multiple pairs of mm-wave transmitter (TX) and receiver (RX). As recently proposed in [2], the frequency bands of interest are the recently commercialized *E*-band (71–86 GHz) and the two higher frequency bands, *W*-band (92–114.25 GHz) and *D*-band (130–148 GHz). Beyond the realization of a point-to-point multiband mm-wave link, the frequency synchronization of these systems situated either at the same or different locations would enable more advanced applications, e.g., ultra-dense mm-wave networks [3], distributed beamforming [4], coordinated and distributed multiple-input and multiple-output (MIMO) [5], cooperative radios [6], and distributed sensing [7]. Nevertheless, the cost associated with realizing such a system and the technical challenge of synchronizing the mm-wave sources in the different bands impose a significant challenge. This is further exacerbated by the difficulty of realizing an mm-wave source directly at its fundamental frequency, and a frequency multiplier is typically used to upconvert a lower frequency source instead. As a frequency multiplier degrades the phase noise by a function of the multiplication factor [8], the phase performance premultiplication must be exceptional. This is a significant constraint, given that the wideband phase noise of an mm-wave source is proposed to be one of the main limiting attributes to the system performance [9], thus entailing the requirement and the mechanism of the distribution of mm-wave sources with good phase noise performance [10].

This work is an extension of the work done in [11], which presented a proof-of-concept experimental demonstration of a multiband mm-wave system architecture at 100- and 112.5-GHz over-the-air, whereby multiple pairs of mm-wave TXs and RXs, operating in different frequency bands and located either at the same or different locations, require only a single oscillator source to generate the corresponding synchronized local oscillator (LO) sources. To achieve this, an unfiltered optical frequency comb (o-comb) with a fine frequency resolution of 1.5625 GHz, was generated using the electrooptic method [12]. With this approach, only one electrical oscillator source, determining both the frequency spacing between the comb tones and the phase noise [13], is required. Using a photodiode (PD), the o-comb is subsequently converted to the corresponding electrical comb (e-comb) for source extraction. The generation of the o-comb can either be done locally (at the mm-wave TXs or RXs site, et al. [14] demonstrated an integrated solution) or distributed through optical fiber to multiple locations, as already demonstrated

Manuscript received 9 July 2023; revised 6 September 2023; accepted 13 October 2023. This work was supported in part by the Royal Society under Grant RGSR1221215, in part by the Engineering and Physical Sciences Research Council (EPSRC) under Grant ORBITS EP/V051377/1, and in part by the EPSRC under Grant TRACCS EP/W026252/1. The work of Dhecha Nopchinda was supported by the Leverhulme Trust under Grant ECF-2020-113. This article is an expanded version of the work presented at the IEEE MTT-S International Microwave Symposium (IMS 2023), San Diego, CA, USA, June 11–16, 2023 [DOI: 10.1109/LMWT.2023.3266815]. *(Corresponding author: Dhecha Nopchinda.)*

Dhecha Nopchinda was with the Department of Electronic and Electrical Engineering, University College London, WC1E 7JE London, U.K. He is now with Gotmic AB, 411 33 Gothenburg, Sweden (e-mail: dhecha@ieee.org).

Zichuan Zhou, Zhixin Liu, and Izzat Darwazeh are with the Department of Electronic and Electrical Engineering, University College London, WC1E 7JE London, U.K. (e-mail: zichuan.zhou.14@ucl.ac.uk; zhixin.liu@ucl.ac.uk; i.darwazeh@ucl.ac.uk).

Color versions of one or more figures in this article are available at https://doi.org/10.1109/TMTT.2023.3326511.

Digital Object Identifier 10.1109/TMTT.2023.3326511

with 22 km of standard single-mode fibers (SSMFs) and compared against commercially available oscillator solution [11]. In addition, the method to synchronize between the TXs or RXs with access to the comb and the corresponding remote RXs or TXs was also demonstrated by broadcasting one of the lower frequency tones, from the e-comb, at 6.25-GHz over-the-air, thus eliminating the need for the TX–RX clock synchronization via global positioning system (GPS) or other means [15], [16], further reducing the carrier recovery requirement and the complexity thereof.

In parallel to radio-over-fiber (RoF) systems [17], [18], the generation of sources at mm-wave and THz frequencies from o-combs is well-studied. However, existing works [19], [20], [21], [22] focus on the realization of state-of-the-art frequency stability and phase noise performance of a single-frequency source, mainly for instrumentation or distribution [10]. In such a case, the o-comb is filtered to extract two of the comb lines. After photodetection, the beating products then result in the wanted LO source at a single frequency. This is in contrast to the technique demonstrated in [11] and studied in this work. By not filtering the o-comb, the counterpart e-comb is directly generated. This allows each frequency-synchronized tone to be extracted and used as needed by simple processing (filtering) of the e-comb at the TX or the RX. Directly generating the e-comb is an attractive technique because, to achieve this property with the established filtered o-comb or single-tone generation techniques, the o-comb will have to be processed in the optical domain, adding significant overhead. Optical splitters, filters, and PDs will be needed for each of the electronic sources to be extracted. Doing so will also further reduce the distributed optical power at the front of the processing chain before photodetection. At a conceptual level, the unfiltered o-comb distribution architecture in this work can be considered as providing multiple locations and systems therein with access to a harmonic frequency synthesizer generating a predetermined set of synchronized frequencies with good phase noise properties. In [23] and [24], the technique to generate the electrooptic comb was described, allowing the distribution of RF tones with 5-GHz spacing. However, only a showcase experimental demonstration was done at a single center frequency of 25 GHz, generated from a single sideband filtered o-comb. Simultaneous multiband transmission and the analysis of the comb performance were not included.

By building upon [11], this work aims to serve as a complete guide to the o-comb distribution and e-comb extraction technique in the context of a multiband mm-wave system. Proposing as a parameter of interest of this technique, significant consideration is given to the effects of the chromatic dispersion of optical fibers on the performance of the resulting sources. To achieve this, a new experimental setup has been built in contrast to the setup in [11], which was designed to demonstrate the efficacy of the architecture for dual-band mm-wave transmission. As will be experimentally demonstrated, the chromatic dispersion of the optical fiber affects both the power and the phase noise of each tone in the e-comb and, subsequently, the extracted sources. By varying the total effective dispersion, either through the length of the SSMF or the usage of dispersion compensating fibers (DCFs), the mm-wave system performance is characterized both at the source and system levels. For the former, the power and phase noise of the extracted sources are measured. For the latter, effects on system-level metrics, including the error vector magnitude (EVM) and the bit-error rate (BER), are considered. Comparisons to two commercially available oscillators and the implementation penalty of the technique are also given under the same methodology.

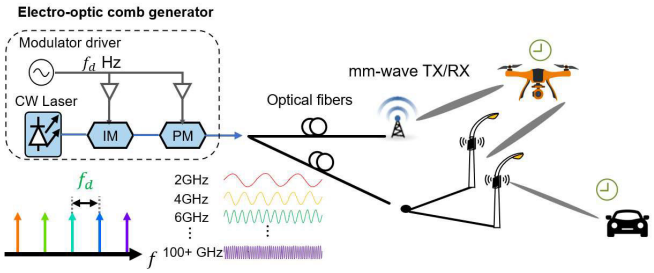

Fig. 1. Simplified conceptual diagram of the comb distribution architecture with the electrooptic comb generator.

This article is organized as follows. The method to generate the o-comb and the relevant theory behind the comb distribution are in Section II. Section III describes the experimental setup designed to characterize the effect of chromatic dispersion. Section IV contains the measurement results, both at the source level (power and phase noise) and the system level (EVM and BER). The work is concluded in Section V.

II. Optical Comb Generation and Distribution

A simplified conceptual diagram of the o-comb generation and distribution architecture is shown in Fig. 1. The o-comb is generated using the electrooptic method and subsequently distributed to multiple locations. At each location, the o-comb is converted to the corresponding e-comb. The source is then extracted at the required frequency to be used in mm-wave TXs or RXs and for different applications as illustrated.

A. Electrooptic Comb Generation (Theory)

The electrooptic comb generator is shown in the top-left corner of Fig. 1. A continuous-wave (CW) seed laser is modulated by an intensity modulator (IM) and a phase modulator (PM), both driven by an electrical oscillator, the comb driver. The IM acts to flatten the comb intensity profile using a flat-top pulse [25], while the PM serves to generate the o-comb itself. Considering only the PM for simplicity, the resulting optical field can be expressed as [26]

$$E_o(t) = E_i \exp\left(j2\pi \upsilon_s t + j\frac{\pi V}{V_\pi}\sin(2\pi f_d t)\right) \tag{1}$$

where E_i is the input optical field amplitude, V is the driving voltage of the PM with a π-phase shift voltage of V_π, f_d is the frequency of the electronic oscillator acting as the comb driver, and υ_s is the seed laser frequency, corresponding to the optical wavelength. Equation (1) can be expressed in the optical frequency domain as [26]

$$E_o(\upsilon) = E_i \sum_{n=-\infty}^{\infty} J_n\left(\frac{\pi V}{V_\pi}\right)\delta(\upsilon - nf_d - \upsilon_s). \tag{2}$$

The term J_n is the Bessel function of the first kind of the nth comb line order. Importantly, the term $\delta(v - nf_d - v_s)$ represents the different comb lines. In practice, the number of comb lines, N, and their output power depend on the ratio between the driving voltage V and V_π of the PM. As for the IM, its driving and bias voltages are simply fine-tuned to get the optimum o-comb intensity envelope.

As observed in (2), the frequency spacing between adjacent comb lines (the comb resolution) is determined by the frequency of the comb driver. Furthermore, if the linewidth of the seed laser is sufficiently small, the phase noise of the comb driver will be the limiting phase noise of the o-comb, dependent on the comb line order [27], [28], [29], [30].

B. Optical Comb Distribution

As shown in Fig. 1, the generated o-comb is distributed via optical fibers to multiple sites with mm-wave TXs or RXs. A PD at each site then converts the o-comb to the corresponding e-comb without prior filtering. As the o-comb travels through SSMFs, three main mechanisms of the fiber will affect the o-combs received at each site: the loss, the nonlinearity, and the chromatic dispersion. The fiber loss is mitigated through the use of an optical amplifier, e.g., an erbium-doped fiber amplifier (EDFA). The nonlinearity is minimized through the careful control of the o-comb launch power into the fiber. The last mechanism, the chromatic dispersion, though can be mitigated using DCFs, is interesting to study as it affects both the magnitude and the phase noise of the distributed unfiltered o-comb and subsequently the corresponding e-comb in a unique way [31].

The effect of chromatic dispersion on the generated single-tone source from a filtered o-comb (two-optical-tone and carrier beating) is studied in [32]. As the dispersion creates a differential delay between the two optical tones and the optical carrier, after beating at the PD, the power of the generated source is found to be fading periodically as a function of the total dispersion or, equivalently, the length of an SSMF (see Fig. 3 in [32]). A general expression for the e-comb photocurrent, including the effect of the chromatic dispersion, is derived in [33]. The results also exhibit the periodic fading profile as the fiber length varies (see Fig. 4 in [33]). For the purpose of discussing the results in this work, the general expression in [33] is simplified. At the PD, the approximate expression of the beating products between N o-comb tones, generating the e-comb, is

$$I(t) = \sum_{n=2}^{N}\sum_{k=1}^{n-1} A_n A_k \cos\Bigg(2\pi(n-k)f_d t + \frac{\pi c}{v_s^2}\left(n^2-k^2\right)f_d^2 DL + \Delta\phi_{n,k}(t)\Bigg). \tag{3}$$

A_n is the amplitude of the nth comb line. c is the speed of light. D is the fiber dispersion parameter (a constant depending on the fiber specification). L is the fiber length. $\Delta\phi_{n,k}(t)$ is the phase difference between the beating nth and kth o-comb lines, containing the phase noise terms of both lines and the initial phase condition. From [30], if the seed laser linewidth is sufficiently narrow, the phase noise of the nth comb line can be approximated to

$$\phi_n(t) \approx n\phi_d(t) \tag{4}$$

where $\phi_d(t)$ is the phase noise of the comb driver. Observing (4) reveals that the phase noise of an o-comb line worsens as the order increases. This represents a physical limitation of the optical comb generation, which can be addressed by minimizing the phase noise of the comb driver. Cost-wise, this approach is suitable for the proposed architecture as the performance of a single comb driver can be utilized at all the distributed locations and frequencies.

The first phase term in (3), $2\pi(n-k)f_d t$, shows the generation of the ith e-comb line: $i = n - k$. As there are multiple pairings of n and k resulting in the same i, it can be seen that the lower order e-comb line is generated from multiple pairs of o-comb beating products, while the highest order e-comb line is generated only from the beating between the highest and the lowest o-comb lines. The second phase term, $\pi c(n^2 - k^2)f_d^2 DL/v_s^2$, reveals that the chromatic dispersion of the fiber creates the periodic fading effect and fluctuation of the e-comb line amplitude as a function of L, the fiber length.

In terms of phase noise, contained within the last phase term, $\Delta\phi_{n,k}(t)$, the chromatic dispersion creates an additional differential delay between the beating o-comb tones (and their phase noise), that is, with a certain fiber length, the phase noise between the o-combs can add up constructively or destructively, affecting the phase noise of each e-comb line. Existing literature has studied the effect of chromatic dispersion on the phase noise for a single source generation but not for the direct generation of e-comb. The work in [31] presented an experimental demonstration of the effect of chromatic dispersion on the phase noise of a single-frequency generation in mm-wave intensity-modulated RoF systems, characterized through the reduction in peak power spectral densities (PSDs). However, deriving the general expression for the phase noise of the e-comb lines generated from an unfiltered o-comb is not a trivial task and is out of the scope of this work, especially as the initial phase condition of each o-comb line is not well-defined and measured experimentally. Nevertheless, we will merely use the above remark to support the experimental results in this work.

III. Experimental Setup

An experimental mm-wave testbed, representing a scenario of W-band transmission with two pairs of TXs and RXs in different subbands (denoted W1 and W2), was built. The W1 and W2 TXs have access to the o-comb, generated OFF-site and distributed through an SSMF, as simplified and shown in Fig. 2. The W1 and W2 RXs are remote and do not have access to the o-comb, as also shown in Fig. 2. The photograph of the setup is shown in Fig. 3. The setup is modified from the wireless setup in [11]. In essence, the setup in [11] was designed to characterize the performance of the architecture at varying mm-wave distances over-the-air, while the setup in this work provides a controlled mm-wave environment to characterize the performance at varying optical

TABLE I
OPTICAL FIBERS TESTED IN THIS WORK

Fiber	SSMF 0 km	SSMF 4 km	SSMF 9km	SSMF 13 km	SSMF 19 km	DCF −19.5 km
Measured Length	21.1 m	4.45 km	8.69 km	13.1 km	19.3 km	3.55 km
Measured Loss (dB)	0	1.8	3	4.5	6.6	1.9

fiber distances and mm-wave attenuation. To achieve this, the W-band antenna pair is replaced with a W-band rotary-vane reading attenuator. The SSMF, which connects the EDFA to the PD, is now variable in length instead of being fixed at 22 km. A variable optical attenuator (VOA) is also included to control the launch power into the different fibers.

A. Overview Description

Observing Fig. 2, the o-comb is generated by the electrooptic comb generator and subsequently amplified optically by an EDFA. The amplified o-comb is then distributed through a varying length of SSMF from 21.2 m (optical back-to-back) to 19 km, as listed in Table I. All SSMFs used in this work have a dispersion parameter of 17 ps/nm/km. A dispersion-compensating fiber (DCF) with a total dispersion of −332 ps/nm was also used as a test point, corresponding to −19.5 km of SSMF. At the mm-wave TXs, the 7-dBm o-comb is converted to the e-comb using a 20-GHz InGaAs P-I-N PD, AR × 20 from APIC Corporation, with 0.95-A/W responsivity. Within the comb processing network in Fig. 2, the e-comb is subsequently amplified, spectrum shown in Fig. 4, split and filtered using three different resonant-cavity bandpass filters (BPFs), and centered at 6.25, 12.5, and 14.0625 GHz, to extract the three corresponding frequency-synchronized tones.

The two latter tones are amplified to 2 dBm and passed through frequency octuplers (×8), generating LO sources at 100 and 112.5 GHz for the W1 and W2 TXs, respectively. The two TXs upconvert and amplify two independent sets of baseband I and Q signals generated by the two arbitrary waveform generators (AWG-1 and AWG-2: Keysight M8190A and Rohde and Schwarz SMW200A, respectively). The W-band signal is transmitted in a back-to-back manner through an instrument-grade rotary-vane reading attenuator (Flann WR10 27110) with the attenuation range of 0–60 dB.

The former tone at 6.25 GHz, inherently frequency synchronized to the 100- and 112.5-GHz LO sources, is used as a reference source for synchronization between the two AWGs. This is done by frequency-dividing the tone to 50 MHz, a division factor of 125, using a modified Hittite HMC983LP5E (loop bandwidth of 87 kHz). In addition, the 6.25-GHz tone is also amplified and broadcasted over-the-air using a WIFI dipole antenna. 6.25 GHz was chosen due to the lower propagation loss, the associated component cost, and the available components, but other e-comb tones can be used.

At the RX side, observing Fig. 2, the broadcasted 6.25 GHz is received and frequency divided, providing a 50-MHz reference signal to the two signal generators (LO-RX 1 and LO-RX 2: R&S SMB100A and SMF100A, respectively) and oscilloscope (Scopes 1 and 2: R&S FSW). The 2-dBm signals from LO-RXs 1 and 2 are frequency multiplied by ×8 and used as LO signals for the W1 and W2 RXs, respectively. Thus, the LO signals of the four W-band TXs and RXs, the AWGs, and the Scope are all frequency-synchronized. The transmitted W-band signals are received and downconverted to baseband and subsequently captured by Scopes 1 and 2.

B. Electrooptic Comb Generator (Experimental Setup)

The o-comb is generated by using the electrooptic method, as shown in Fig. 2 (top-left corner). The photograph of the o-comb generation setup is shown in Fig. 5. A 10-dBm output power 100-Hz linewidth CW seed laser at 1555 nm is modulated with a PM driven by a low-noise 1.5625-GHz tone, generated by Signal Core SC5511A (phase noise: −137 dBc/Hz at 10-kHz offset from 1 GHz). The output of the PM is directly fed into an IM driven by the same RF tone. The ultranarrow linewidth laser satisfies the approximating condition in (4). After photodetection, the extracted tones, circled in red in Fig. 4, at 6.25, 12.5, and 14.0625 GHz are therefore the 4th-, 8th-, and 9th-order harmonics, respectively.

C. W-Band TXs and RXs

The fully integrated W1 and W2 TXs and RXs are from Gotmic AB using the GaAs pHEMT technology. The two pairs have recently been characterized and reported in [2] with two alterations: the W2 TX has been improved with a higher-output-power power amplifier (PA) and the W1 RX is without the integrated IF amplifier.

The TXs are mainly equipped with an 8× in the LO path, a differential IQ mixer, and a PA. W1 and W2 TXs have RF bandwidths of 86–102 and 94–116 GHz and output 1-dB compression points (P1dB) of 24 and 17.5 dBm, respectively. The RXs include an 8×, a differential IQ mixer, a low-noise amplifier, and an IF amplifier for the W2 RX. W1 and W2 RXs have RF bandwidths of 88–102 and 100–115 GHz and third-order input-intercept points of 1 and 2 dBm, respectively.

D. Baseband TXs and RXs

At the TXs, the two AWGs operating at a 2.4-GHz sampling rate are generating baseband signals from two independent baseband TXs, implemented in MATLAB. The baseband signals are 16-QAM OFDM with 34 subcarriers at 3.2 Gbit/s per TX. At the RXs, the baseband signals captured by Scopes 1 and 2 are processed offline using baseband RXs implemented in MATLAB. The OFDM RXs include standard framing and timing synchronization, and detection. No channel equalization was performed as the rotary-vane attenuator provides a controlled mm-wave environment and also no frequency correction or carrier recovery as this was facilitated by the broadcasted reference source from the e-comb at 6.25 GHz.

IV. RESULTS

A. Measured Source Power With Different Fiber Lengths

The power of the extracted sources at three different frequencies of interest (6.25, 12.5, and 14.0625 GHz) was

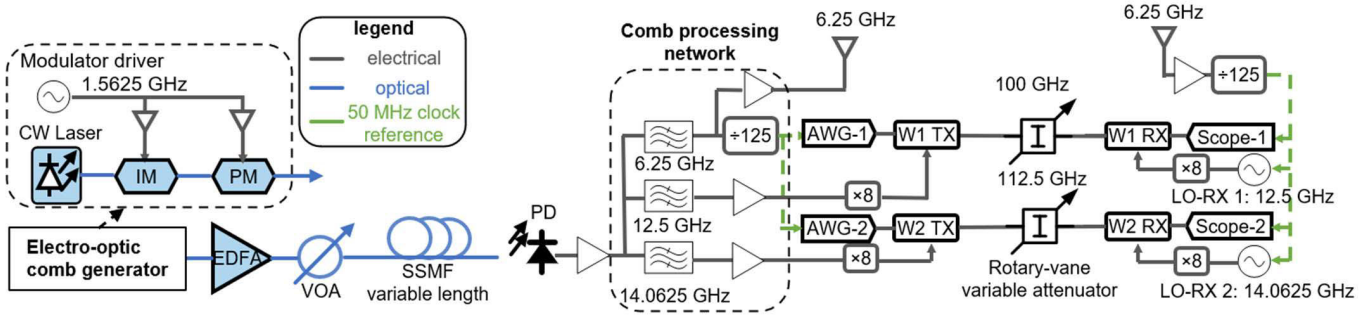

Fig. 2. Simplified block diagram of the experimental setup.

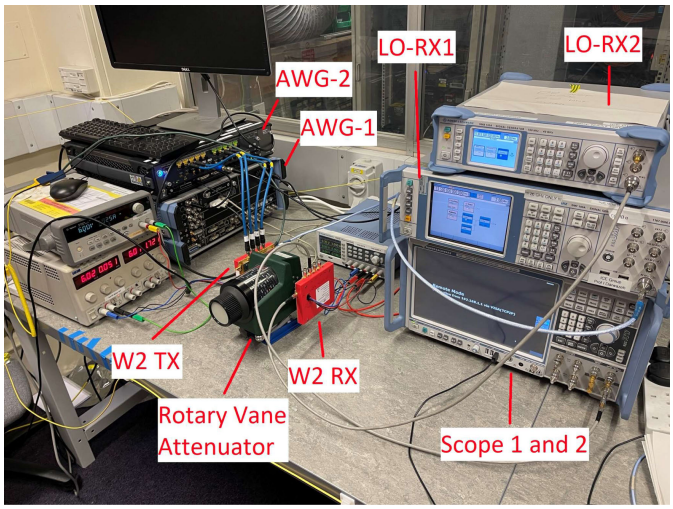

Fig. 3. Photograph of the experimental setup. A rotary-vane attenuator was used to provide a controlled W-band channel.

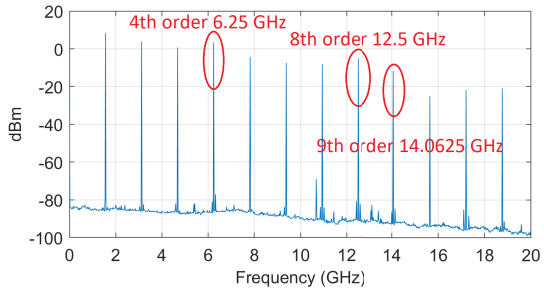

Fig. 4. Spectrum of the generated e-comb with 9 km of SSMF.

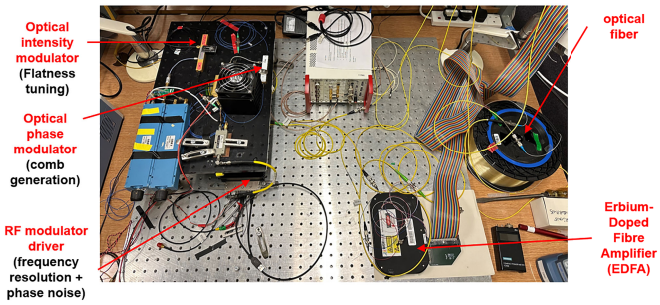

Fig. 5. Photograph of the experimental setup generating the o-comb. The length of the optical fiber is varied, changing the chromatic dispersion as a parameter of interest.

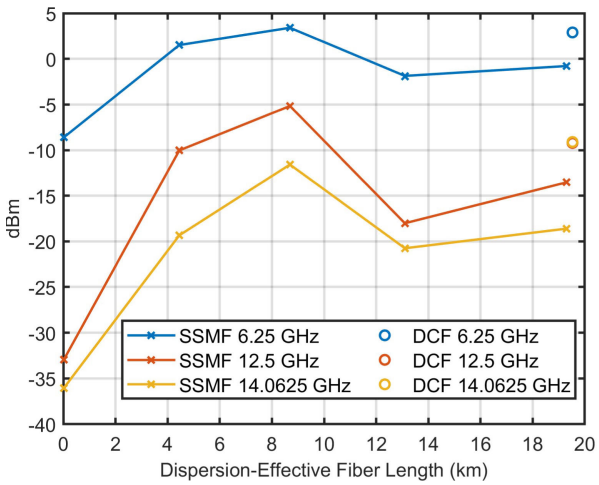

Fig. 6. Measured power of the comb-extracted source at three different frequencies at varying SSMF length. The chromatic dispersion of the DCF corresponds to −19.5 km of SSMF.

measured as a function of the SSMF length, as shown in Fig. 6. An additional set of measurements was also performed with the DCF with a negative dispersion value corresponding to 19.5 km length of SSMF. Multiple observations can be made with Fig. 6.

First, the power of the extracted source is a function of its frequency. The lowest frequency source at 6.25 GHz exhibits the highest power, regardless of the fiber length, while the highest frequency source at 14.0625 GHz exhibits the lowest. This agrees with (3) and the corresponding remark in Section II; the lowest order tone (6.25 GHz is the fourth order) is a summation of a larger number of beating products relative to the highest order (14.0625 GHz is the ninth order). This also explains why the power of the 12.5-GHz tone (eighth order) is close to that of 14.0625 GHz.

Second, the power of each frequency source exhibits fading and fluctuates as a function of the fiber length. This again agrees with (3) and the remark in Section II, where it was shown that the chromatic dispersion creates power fading as a function of the fiber length.

Third, the DCF agrees well with the SSMF at the same dispersion-effective fiber length. The small discrepancies are mostly attributed to the higher nonlinearity of a DCF, relative to an SSMF.

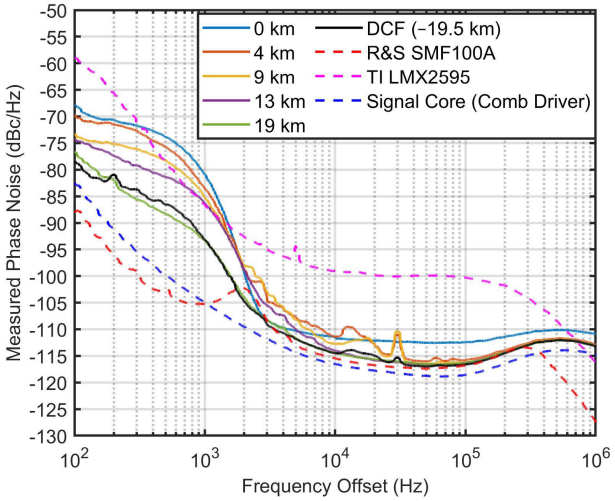

Fig. 7. Measured phase noise of the 14.0625-GHz comb-extracted source as a function of offset frequency at varying SSMF length, including DCF. Two commercially available oscillators along with the o-comb driver are also included.

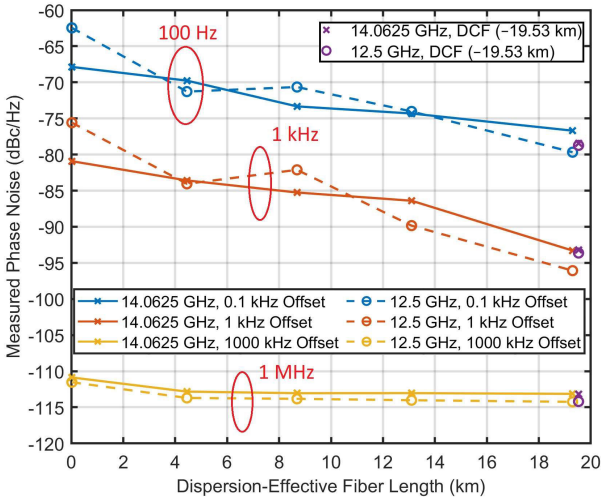

Fig. 8. Measured phase noise of the comb-extracted sources at 12.5 and 14.0625 GHz as a function of the dispersion-effective SSMF length. For each length, the phase noise was measured at 100-Hz, 1-kHz, and 1-MHz offsets.

Finally, perhaps counterintuitively, the extracted source power does not overall decrease as the fiber length increases. This is because the VOA (see Fig. 2) was used to control the launch power of the o-comb into the fiber such that the average received o-comb power is 7 dBm, in conjunction with the limited length of fiber used in this work (maximum 19.3 km), corresponding to a smaller value of fiber attenuation as measured in Table I. This means that the limiting effect on the extracted source power is the chromatic dispersion and not the loss of the fiber itself.

B. Measured Phase Noise With Different Fiber Lengths

To study the effect of the fiber distribution, with each SSMF length, and hence the corresponding chromatic dispersion, the phase noise of the LO sources extracted from the e-comb is measured using R&S FSWP phase noise analyzer. Fig. 7 shows the measured phase noise of the comb-extracted source at 14.0625 GHz at varying fiber lengths in solid lines. The result with the DCF instead of the SSMF is also included. The phase noise of three different oscillators is also measured and shown with the dashed lines: R&S SMF100A, TI LMX2595, and the Signal Core SC5511A (o-comb driver). The R&S SMF100A and the TI are included to compare the comb-extracted sources with commercially available synthesizers. The R&S SMF100A is an instrument-grade testbench generator. Meanwhile, the TI is used to represent an integrated solution covering the same frequency range of 20 GHz as the PD used in this work. The Signal Core is included to deduct the implementation penalty of the architecture.

Observing Fig. 7, the phase noise was measured from 100-Hz to 1-MHz offset frequency. Multiple observations can be made.

First, the measured phase noise of the comb-extracted sources depends on the distribution SSMF lengths, to be discussed further using Fig. 8.

Second, similar to the measured power, the measured phase noise with the DCF agrees with that of 19-km SSMF. As the DCF and the 19-km SSMF have different nonlinearity, loss, and physical length (see Table I), this further indicates that the measured phase noise of the comb-extracted sources in this setup is largely dependent on the total chromatic dispersion as remarked with (3) in Section II.

Third, against the TI LMX2595, at all fiber lengths, the proposed method performed better in the near-carrier region below 300-Hz offset but exhibited a slight disadvantage from 300 Hz to 1.5 kHz with 0- and 4-km SSMFs, beyond which, the comb performs significantly better. Against the test bench R&S, the comb exhibits disadvantages in the near-carrier region and up to 2 kHz. Beyond that, the performance is largely similar. Against the signal core and its driving source, the comb exhibited expansion of the phase noise in the region below 30 kHz. This is an anticipated effect from the beating product and the phase noise of the o-comb in (3) and (4), that is in the optical domain, the near-carrier phase noise of the nth o-comb line is expanded by approximately n times, similar to a behavior of a frequency multiplier [14]. The observed e-comb phase noise is then the amalgamation of the beating products of these expanded o-comb lines as in (3). However, the wideband phase noise performance in the >30-kHz region matches closely with the low phase noise of the driver, including the hump observed between 100-kHz and 1-MHz offsets. The wideband phase noise performance makes the architecture suitable for wideband mm-wave transmission.

The measured phase noise at 100-Hz, 1-kHz, and 1-MHz offsets of the comb-extracted sources at both 12.5 and 14.0625 GHz is shown as a function of the SSMF length in Fig. 8. Agreeing with the original results in [11], the performance difference between 12.5 and 14.0625 GHz is marginal. This is as expected due to the low-order difference between the eighth- and the ninth-order tones and its effect in (4), similar to what was observed with the power of both sources. At a 1-MHz offset, the wideband phase noise is observed to be independent of the fiber length. However, the near carrier, at 100 Hz and 1 kHz, is observed to be decreasing as the

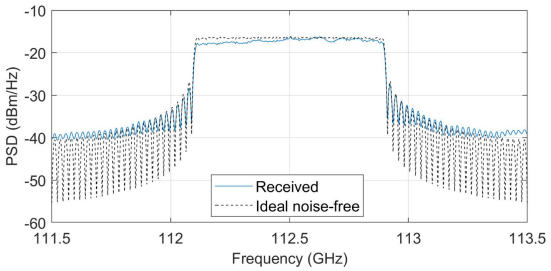

Fig. 9. Received PSD at 26-dB W-band attenuation and 9-km SSMF along with those of ideal noise-free signals as reference.

SSMF length increases and the phase noise on each o-comb line becomes decorrelated. Again, the agreement between the DCF and the 19-km SSMF is further shown in Fig. 8.

As the general expression for the relationship between the e-comb phase noise and the chromatic dispersion was not present, this set of results does not indicate in general that the phase noise of an e-comb-extracted source decreases as the fiber length increases. The results and the corresponding analysis merely experimentally demonstrate that the optical fiber, through its chromatic dispersion mechanism, affects the resulting phase noise performance of the extracted sources.

C. Data Transmission (System-Level Characterization)

To demonstrate the effect of the chromatic dispersion on the system performance, data transmission experiments were performed through the instrument-grade rotary-vane attenuator, shown in Figs. 2 and 3, providing a controlled mm-wave environment. At each SSMF length (see Table I), the W-band attenuation was varied between 12 and 40 dB with a 2-dB step size. The attenuation range corresponds to the free-space path loss in W2 (at 112.5 GHz) of 0.8–21.2 m, assuming a 30-dB gain in each of the TX and RX antennas. As the W1 TX exhibits a strong frequency roll-off from the PA (see Fig. 5 in [11] and Fig. 4 in [2]), in conjunction with the observation that the 12.5- and 14.0625-GHz sources perform largely similarly, only the performance of the W2 TX-RX pair was characterized to make way for a clear observation of the effect the chromatic dispersion. The system performance was characterized using the EVM, the BER, the measured differential phase noise variance, and the symbol constellation.

Carrying 4 406 400 bits, the W2 received PSD at 26-dB attenuation and 9-km SSMF length is shown in Fig. 9, along with the PSD of the ideal noise-free signal as a reference. The received EVMs at different W-band attenuation levels and SSMF lengths are shown in Fig. 10. In terms of the latter, the measured EVM is observed to decrease as the SSMF length increases. This agrees with the lower near-carrier phase noise at higher SSMF lengths, as shown in Fig. 8. Simultaneously, the W-band attenuation level reveals the RX noise and the RX distortion limited regions, as shown in Fig. 10. The lowest EVM of 12% is observed with 26-dB attenuation and 19-km SSMF. At the system level, the effect of the SSMF length in the RX distortion limited region is not observable as the performance is limited by the nonlinearity. This is further verified by observing Fig. 11, showing the received average

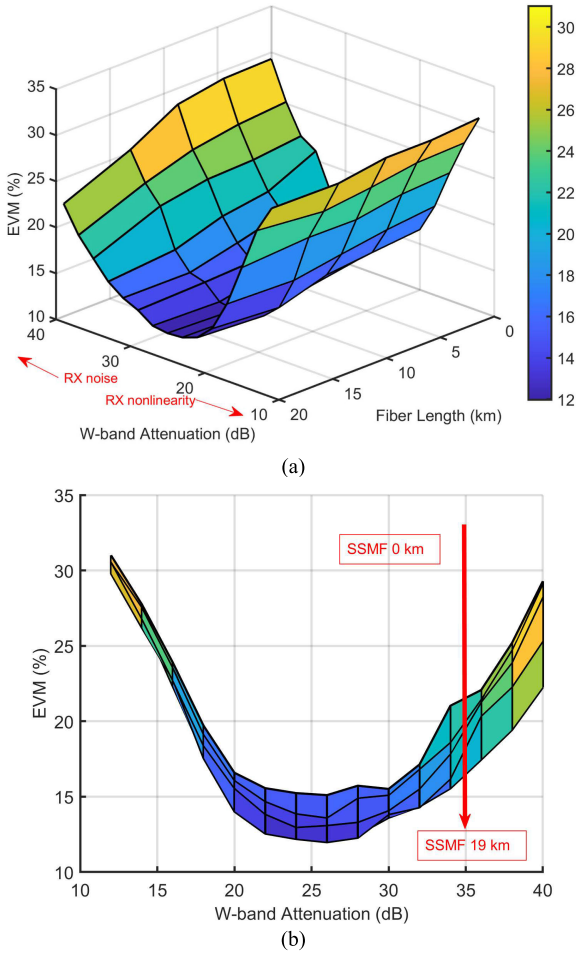

Fig. 10. Experimentally obtained EVM as a function of both the W-band attenuation and SSMF length. (a) Top view. (b) Side view.

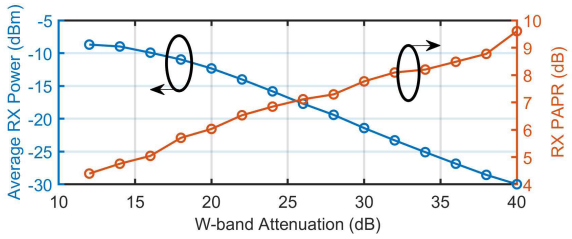

Fig. 11. Measured average received power and PAPR at varying W-band attenuation and 9-km SSMF. The transmitting PAPR is 11.3 dB.

power and the received peak-to-average power ratio (PAPR) at varying W-band attenuation and 9-km SSMF. By comparing with the transmitting PAPR of 11.3 dB, the distortion and noise regions of the RX can be observed.

The above observations are further supported by the measured BER results shown in Fig. 12. In the same manner as the EVM, Fig. 12(a) shows that the BER is a function of both the W-band attenuation and the SSMF length. The BER decreases as the fiber length increases. Error-free (lower than the statistical confidence) levels are observed at higher fiber lengths outside of the noise and distortion limited regions. Fig. 12(b), which also shows the 100-bit error level, reveals that the BER performance can be significantly affected by the fiber length outside of the noise and distortion limited region

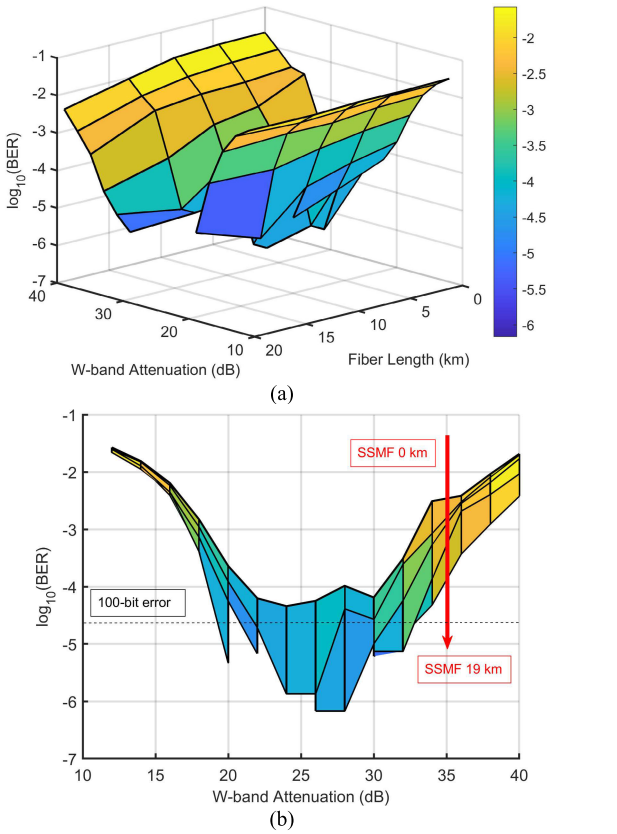

Fig. 12. Experimentally obtained BER as a function of both the W-band attenuation and SSMF length. (a) Top view. (b) Side view.

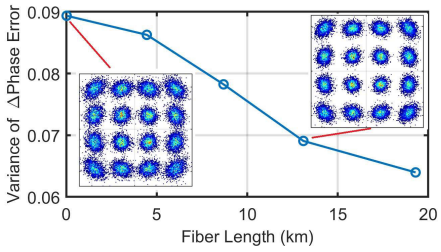

Fig. 13. Measured variance of the differential phase error. Averaged across subcarrier (frequency) and W-band attenuation, along with two corresponding symbol constellations at 112.82 GHz and 26-dB W-band attenuation.

(between 20- and 30-dB W-band attenuation). Furthermore, by comparing the spread of the BER in the distortion limited region (12–20-dB attenuation) and the noise limited region (30–40-dB attenuation), it can be observed that the SSMF length influences the BER in the noisy region much more than the nonlinear region, agreeing with the EVM results.

To characterize the phase noise at the system level, the variance of the differential phase error (the development of the phase error between each symbol, akin to the variance of the noise term in the Wiener phase noise model [34]) is measured across all 34 subcarriers, averaged across the subcarriers and W-band attenuation levels and is shown in Fig. 13. The variance decreases as the SSMF length increases, further corroborating the prior results. To illustrate, the constellation diagrams at 26-dB W-band attenuation of the 17 even subcarriers as a function of frequency, along with that of

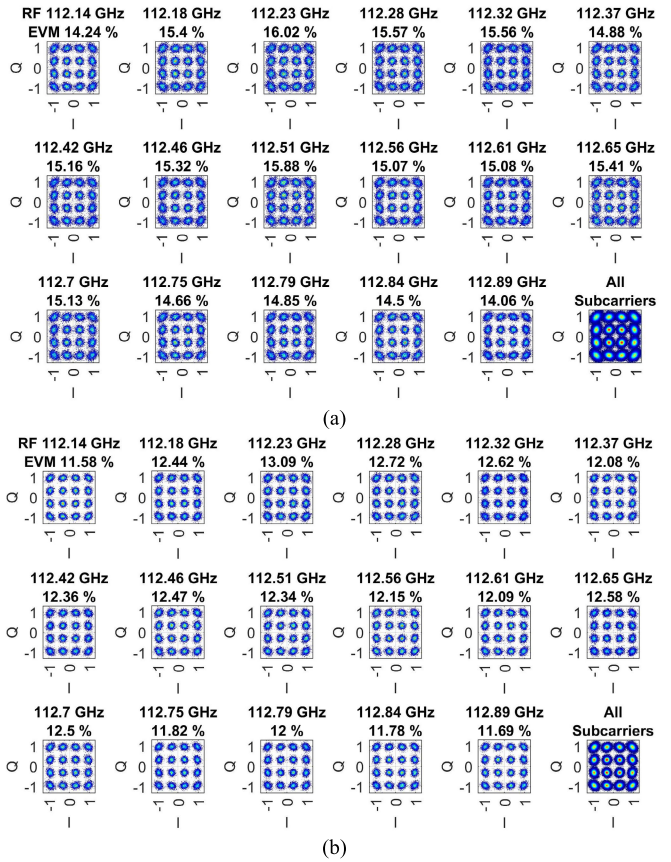

Fig. 14. Received constellation diagrams of the even subcarriers at 26-dB W-band attenuation with the corresponding EVM and RF, at different SSMF lengths. (a) 0 km. (b) 19 km.

all subcarriers, are shown in Fig. 14. Fig. 14(a) and (b) corresponds to the SSMF lengths of 0 and 19 km, respectively. Differences in the received symbol constellations under the two fiber lengths can be observed.

All these system-level characterizations demonstrate that the chromatic dispersion, determined through the length of the SSMF, can have an observable and, in some scenarios, significant impact on the performance of the architecture.

V. Conclusion

The performance of the proposed mm-wave system architecture has been studied and experimentally demonstrated. In this architecture, simultaneous data transmission in different mm-wave frequency bands can be achieved using a single oscillator to generate an optical comb. The optical comb is then distributed to multiple locations, where the corresponding e-comb with a fine frequency resolution is generated. As all the tones in the e-comb are frequency-synchronized, the required frequency source for each mm-wave TX can then be extracted as needed. A lower frequency source was also broadcasted over-the-air to provide frequency synchronization to a remote location, e.g., the mm-wave RXs, thus eliminating the need to provide frequency synchronization by other existing techniques. Ultimately, the architecture provides a method to utilize a single electronic oscillator with good phase noise properties and, perhaps costly, in two different dimensions of

location and frequency, with the inherent frequency synchronization capability being another benefit.

The chromatic dispersion of the optical fiber used to distribute the optical comb, principally determined by the fiber's length for an SSMF, is proposed as an important parameter to the performance of the extracted source. The theoretical justification to support this statement is presented and used to support the experimental results. The power and the phase noise of the extracted tones were measured at varying fiber lengths, and dependency was observed through the power-fading and the differential delays resulting from the dispersion. A DCF, with the total dispersion comparable to that of one of the standard fiber lengths, was also included as a test point. Comparable performance, in both power and phase noise, between the two fibers is observed, further supporting the importance of the chromatic dispersion. The measured set of phase noise (of the extracted tones) was also compared against those of two commercially available oscillators (one integrated and one test bench) and also the oscillator used to generate the comb. Only a slight penalty in the frequency region close to the carrier results from this implementation, and no penalty was observed in the region further away. The effect of the chromatic dispersion was also demonstrated at the system level through various metrics, including the EVM and the BER. The varying fiber lengths are observed to have a direct impact on the system performance, agreeing with the source-level characterization. In practice, to combat the dispersive effect, a liquid crystal on silicon photonic processor (including some wavelength-selective switches or a Waveshaper), such as that used in [35] to address the power fading issue for single-tone generation, may be utilized at each distributed location to independently control the phase of each o-comb line in order to optimize the resulting power fading and phase noise performance according to the set of frequencies needed at that location.

The architecture provides an effective and scalable solution to the mm-wave phase noise challenge, e.g., the 11th-order harmonic at 17.1875 GHz in the demonstrated electronic comb can be used with a frequency octupler to generate an additional frequency-synchronized source at 137.5 GHz in the *D*-band. Furthermore, with the increasing commercial availability of high-frequency PDs, multiple mm-wave tones may be generated based on this technique directly, foregoing the requirement of a frequency multiplier, ultimately enhancing the phase noise performance. However, as is the main message of this work, care must be taken on the optical fibers used in deployment to ensure optimal system performance.

REFERENCES

[1] A. Dogra, R. K. Jha, and S. Jain, "A survey on beyond 5G network with the advent of 6G: Architecture and emerging technologies," *IEEE Access*, vol. 9, pp. 67512–67547, 2021.

[2] M. Hörberg et al., "A W-band, 92–114 GHz, real-time spectral efficient radio link demonstrating 10 Gbps peak rate in field trial," in *IEEE MTT-S Int. Microw. Symp. Dig.*, Denver, CO, USA, Jun. 2022, pp. 545–548.

[3] R. G. Stephen and R. Zhang, "Joint millimeter-wave fronthaul and OFDMA resource allocation in ultra-dense CRAN," *IEEE Trans. Commun.*, vol. 65, no. 3, pp. 1411–1423, Mar. 2017.

[4] R. Mudumbai, D. R. Brown, U. Madhow, and H. V. Poor, "Distributed transmit beamforming: Challenges and recent progress," *IEEE Commun. Mag.*, vol. 47, no. 2, pp. 102–110, Feb. 2009.

[5] M. Sawahashi, Y. Kishiyama, A. Morimoto, D. Nishikawa, and M. Tanno, "Coordinated multipoint transmission/reception techniques for LTE-advanced [coordinated and distributed MIMO]," *IEEE Wireless Commun.*, vol. 17, no. 3, pp. 26–34, Jun. 2010.

[6] M. K. Karakayali, G. J. Foschini, and R. A. Valenzuela, "Advances in smart antennas—Network coordination for spectrally efficient communications in cellular systems," *IEEE Wireless Commun.*, vol. 13, no. 4, pp. 56–61, Aug. 2006.

[7] C.-Y. Chong and S. P. Kumar, "Sensor networks: Evolution, opportunities, and challenges," *Proc. IEEE*, vol. 91, no. 8, pp. 1247–1256, Aug. 2003.

[8] D. Nopchinda, "OFDM upconverting transmitter using a frequency multiplier," in *Proc. 52nd Eur. Microw. Conf. (EuMC)*, Milan, Italy, Sep. 2022, pp. 20–23.

[9] J. Chen et al., "Influence of white LO noise on wideband communication," *IEEE Trans. Microw. Theory Techn.*, vol. 66, no. 7, pp. 3349–3359, Jul. 2018.

[10] H. Schmuck, R. Heidemann, and R. Hofstetter, "Distribution of 60 GHz signals to more than 1000 base stations," *Electron. Lett.*, vol. 30, no. 1, pp. 59–60, Jan. 1994.

[11] D. Nopchinda, Z. Zhou, Z. Liu, and I. Darwazeh, "Experimental demonstration of multiband comb-enabled mm-wave transmission," *IEEE Microw. Wireless Technol. Lett.*, vol. 33, no. 6, pp. 919–922, Jun. 2023.

[12] N. Kuse and M. E. Fermann, "Electro-optic comb based real time ultra-high sensitivity phase noise measurement system for high frequency microwaves," *Sci. Rep.*, vol. 7, no. 1, pp. 1–8, Jun. 2017.

[13] G. Qi et al., "Phase-noise analysis of optically generated millimeter-wave signals with external optical modulation techniques," *J. Lightw. Technol.*, vol. 24, no. 12, pp. 4861–4875, Dec. 2006.

[14] E. S. Lima, N. Andriolli, E. Conforti, G. Contestabile, and A. C. Sodré, "Low-phase-noise tenfold frequency multiplication based on integrated optical frequency combs," *IEEE Photon. Technol. Lett.*, vol. 34, no. 16, pp. 878–881, Aug. 2022.

[15] M. Ouellette, K. Ji, S. Liu, and H. Li, "Using IEEE 1588 and boundary clocks for clock synchronization in telecom networks," *IEEE Commun. Mag.*, vol. 49, no. 2, pp. 164–171, Feb. 2011.

[16] A. N. Mody and G. L. Stuber, "Synchronization for MIMO OFDM systems," in *Proc. IEEE Global Telecommun. Conf.*, San Antonio, TX, USA, Nov. 2001, pp. 509–513.

[17] X. Pang et al., "Bridging the terahertz gap: Photonics-assisted free-space communications from the submillimeter-wave to the mid-infrared," *J. Lightw. Technol.*, vol. 40, no. 10, pp. 3149–3162, May 2022.

[18] H. Shams et al., "100 Gb/s multicarrier THz wireless transmission system with high frequency stability based on a gain-switched laser comb source," *IEEE Photon. J.*, vol. 7, no. 3, pp. 1–11, Jun. 2015.

[19] D. Wake, C. R. Lima, and P. A. Davies, "Optical generation of millimeter-wave signals for fiber-radio systems using a dual-mode DFB semiconductor laser," *IEEE Trans. Microw. Theory Techn.*, vol. 43, no. 9, pp. 2270–2276, Sep. 1995.

[20] T. M. Fortier et al., "Optically referenced broadband electronic synthesizer with 15 digits of resolution," *Laser Photon. Rev.*, vol. 10, no. 5, pp. 780–790, Sep. 2016.

[21] T. Nakamura et al., "Coherent optical clock down-conversion for microwave frequencies with 10^{-18} instability," *Science*, vol. 368, no. 6493, pp. 889–892, May 2020.

[22] B. T. Bosworth et al., "Electro-optically derived arbitrary millimeter-wave sources with 100 GHz of bandwidth," in *Proc. Conf. Lasers Electro-Opt. (CLEO)*, San Jose, CA, USA, May 2022, pp. 1–2.

[23] Z. Zhou, D. Nopchinda, M.-C. Lo, I. Darwazeh, and Z. Liu, "Simultaneous clock and RF carrier distribution for beyond 5G networks using optical frequency comb," in *Proc. Eur. Conf. Opt. Commun. (ECOC)*, Basel, Switzerland, Sep. 2022, pp. 1–4.

[24] Z. Zhou, D. Nopchinda, I. Darwazeh, and Z. Liu, "Synchronising clock and carrier frequencies with low and coherent phase noise for 6G," in *Proc. IEEE Radio Wireless Symp. (RWS)*, Las Vegas, NV, USA, Jan. 2023, pp. 4–6.

[25] R. Wu, V. R. Supradeepa, C. M. Long, D. E. Leaird, and A. M. Weiner, "Generation of very flat optical frequency combs from continuous-wave lasers using cascaded intensity and phase modulators driven by tailored radio frequency waveforms," *Opt. Lett.*, vol. 35, no. 19, pp. 3234–3236, 2010.

[26] H. Sun, M. Khalil, Z. Wang, and L. R. Chen, "Recent progress in integrated electro-optic frequency comb generation," *J. Semicond.*, vol. 42, no. 4, Apr. 2021, Art. no. 041301.
[27] A. Ishizawa et al., "Phase-noise characteristics of a 25-GHz-spaced optical frequency comb based on a phase- and intensity-modulated laser," *Opt. Exp.*, vol. 21, no. 24, pp. 29186–29194, 2013.
[28] L. Lundberg, M. Mazur, A. Fiilöp, V. Torres-Company, and M. Karlsson, "Phase correlation between lines of electro-optical frequency combs," in *Proc. Conf. Lasers Electro-Opt. (CLEO)*, Washington, DC, USA, May 2018, pp. 1–2.
[29] G. Brajato, L. Lundberg, V. Torres-Company, M. Karlsson, and D. Zibar, "Bayesian filtering framework for noise characterization of frequency combs," *Opt. Exp.*, vol. 28, no. 9, pp. 13949–13964, Apr. 2020.
[30] C. Deakin, Z. Zhou, and Z. Liu, "Phase noise of electro-optic dual frequency combs," *Opt. Lett.*, vol. 46, no. 6, pp. 1345–1348, Mar. 2021.
[31] R. Hofstetter, H. Schmuck, and R. Heidemann, "Dispersion effects in optical millimeter-wave systems using self-heterodyne method for transport and generation," *IEEE Trans. Microw. Theory Techn.*, vol. 43, no. 9, pp. 2263–2269, Sep. 1995.
[32] U. Gliese, S. Norskov, and T. N. Nielsen, "Chromatic dispersion in fiber-optic microwave and millimeter-wave links," *IEEE Trans. Microw. Theory Techn.*, vol. 44, no. 10, pp. 1716–1724, Oct. 1996.
[33] H. H. Elwan, J. Poette, and B. Cabon, "Simplified chromatic dispersion model applied to ultrawide optical spectra for 60 GHz radio-over-fiber systems," *J. Lightw. Technol.*, vol. 37, no. 19, pp. 5115–5121, Oct. 1, 2019.
[34] N. J. Kasdin, "Discrete simulation of colored noise and stochastic processes and $1/f^{\alpha}$ power law noise generation," *Proc. IEEE*, vol. 83, no. 5, pp. 802–827, May 1995.
[35] H. H. Elwan, C. Browning, J. Poette, L. P. Barry, and B. Cabon, "Compensation of fiber dispersion induced-power fading in reconfigurable millimeter-wave optical networks," *Opt. Commun.*, vol. 476, Dec. 2020, Art. no. 126308.

Dhecha Nopchinda (Member, IEEE) was born in Bangkok, Thailand, in 1991. He received the B.Eng. degree (First Class Hons.) in electronic and communication engineering from the Sirindhorn International Institute of Technology, Thammasat University, Pathum Thani, Thailand, in 2013, the M.Sc. degree (with distinction) in wireless and optical communication from University College London, London, U.K., in 2014, and the Ph.D. degree in microtechnology and nanoscience from the Chalmers University of Technology, Gothenburg, Sweden, in 2019.

From 2015 to 2020, he was with the Microwave Electronics Laboratory, Chalmers University of Technology, Gothenburg, Sweden. Funded by the Leverhulme Trust's Early Career Fellowship, he was with the Department of Electronic and Electrical Engineering, University College London, from 2020 to 2023, where he helped setup and managed the mm-wave laboratory and led the mm-wave measurement research work. In 2023, he joined Gotmic, an mm-wave circuit and system design house in Gothenburg, Sweden, as a Microwave System Engineer, where he currently leads the system-level measurements and characterization workgroup. His research interests include digital techniques and signal processing for experimental high-data-rate communication and mm-wave instrumentation.

Dr. Nopchinda was a recipient of a scholarship to study with the Sirindhorn International Institute of Technology from 2009 to 2013, the Leverhulme Trust's Early Career Fellowship from 2020 to 2023, and the inaugural First Place in IEEE Microwave Theory and Technology Society's Early Career Paper Competition at the 2023 International Microwave Symposium.

Zichuan Zhou (Member, IEEE) received the B.Eng. degree in electronic and electrical engineering from University College London, London, U.K., in 2018, and the M.Res. degree in integrated photonic and electronic systems from the University of Cambridge, Cambridge, U.K., in 2019. He is currently pursuing the Ph.D. degree in electronic and electrical engineering at University College London.

His research interests include data center interconnects, radio access networks, passive optical networks, optical frequency comb applications, and low-latency optical transceivers.

Zhixin Liu (Senior Member, IEEE) received the B.Eng. degree in information engineering and the B.B.A. degree in business administration from Tianjin University, Tianjin, China, in 2006, the M.S. degree in electrical engineering from Shanghai Jiao Tong University, Shanghai, China, in 2009, and the Ph.D. degree in information engineering from The Chinese University of Hong Kong, Hong Kong, in 2012.

In 2013, he joined the Optoelectronics Research Centre, University of Southampton, Southampton, U.K. In 2016, he joined the Department of Electronics and Electrical Engineering, University College London, London, U.K. His research focuses on exploring analog and optical signal processing techniques for high-performance communication systems, including high-speed direct modulation, frequency comb, photonic-assisted data conversion, and low-latency data communications.

Dr. Liu is a Senior Member of Optica.

Izzat Darwazeh (Senior Member, IEEE) received the Graduate degree in electrical engineering from the University of Jordan, Amman, Jordan, in 1984, and the M.Sc. and Ph.D. degrees from The University of Manchester, Manchester, U.K., in 1986 and 1991, respectively.

He holds the University of London Chair of communications engineering and leads the 70-Strong Information and Communications Engineering Group, Department of Electronic and Electrical Engineering, University College London, London, U.K., where he is also the Director of the Institute of Communications and Connected Systems. He has authored/coauthored more than 250 articles and book chapters in the areas of optical and wireless communications and monolithic microwave integrated circuits and high-speed/-frequency circuits. He coedited *Analog Optical Fiber Communications* (IEE, 1995) and *Newness Book on Electrical Engineering* (Elsevier) in 2008. He has also coauthored two books *Linear Circuit Analysis and Modeling* (Elsevier in 2005) and *Microwave Active Circuit Analysis and Design* (Academic Press, in 2015). He proposed (with Miguel Rodrigues) the Fast OFDM concept in 2002 and the SEFDM concept in 2003 and has been working on these topics since. He currently teaches mobile and wireless communications and circuit design and his current research activities are in ultrahigh-speed microwave circuits and wireless and optical communication systems.

Dr. Darwazeh is a Chartered Engineer and a Fellow of IET and the Institute of Telecommunications Professionals.